1494

Upconversion, Lifetime Quenching, and Ground-State Bleaching in $Nd^{3+}:LiYF_4$

M. Pollnau, P. J. Hardman, W. A. Clarkson, and D. C. Hanna

Optoelectronics Research Centre
University of Southampton
Southampton SO17 1BJ
United Kingdom
Tel. +44-1703-59 31 41
Fax +44-1703-59 31 42
e-mail mp@orc.soton.ac.uk

Abstract

Since the Nd^{3+}:$LiYF_4$ system has some advantage over Nd^{3+}:YAG and Nd^{3+}:YVO_4 for high-power scaling of diode-end-pumping, this system has been investigated under strong excitation, in this case using a Ti:sapphire pump. The interionic processes responsible for fluorescence saturation have been determined, due allowance being taken for the significant ground-state bleaching under these conditions. Their temperature dependence, which is relevant to scaling consideration, has been investigated theoretically, and found to be rather small over a wide temperature range. By comparing the experimental data with finite-element rate-equation calculations, the influence of interionic upconversion is determined quantitatively, and a published value of the upconversion parameter is confirmed. The spatial dependence of ground-state bleaching and quenching of the fluorescence lifetime is calculated. Analytical expressions are derived, including the influence of interionic upconversion, for the dependence of ground-state bleaching, excitation density, and storage time on pump parameters and dopant concentration.

PACS: 42.55.-f 42.60.Lh 42.70.Hj

Keywords:

Neodymium, Lithium Yttrium Fluoride,

interionic process, upconversion,

lifetime quenching, ground-state bleaching

1. Introduction

The laser transition at ~ 1.05-1.06 μm in Nd^{3+} has been widely investigated and exploited as a classical four-level laser system for 35 years. The pump levels as well as the lower laser level are depleted by fast multiphonon relaxation [1-5], leading to significant excitation solely in the $^4F_{3/2}$ upper laser level. The strong stimulated-emission cross-section allows a low laser threshold, while the small quantum defect allows high slope efficiency. These favorable features have made the near infrared Nd^{3+} laser the solid-state laser of choice for a wide variety of applications which are not wavelength-specific.

In addition to YAG, $LiYF_4$ has also attracted much attention as a host material for Nd^{3+} for various reasons. These include the wavelength match (1.053 μm) with Nd^{3+} glass amplifiers, the long storage time of the Nd^{3+} upper laser level, its natural birefringence, and its relatively weak thermal lensing on the polarization corresponding to 1.053 μm operation. This weak lensing gives Nd^{3+}:$LiYF_4$ a significant advantage over Nd^{3+}:YAG for power-scaling of diode-end-pumped systems into the multiwatt region while retaining an output beam of high spatial quality. Given this interest in Nd^{3+}:$LiYF_4$ it is important to understand and quantify the mechanisms that may play a significant role under intense pumping conditions. Thus, with increasing pump power and intensity, the Nd^{3+}:$LiYF_4$ system has been shown to exhibit a significantly reduced storage time under Q-switched operation and a decreasing laser efficiency [6,7].

Furthermore, measurements of the induced thermal lens under lasing and non-lasing conditions [8-11] demonstrate that significant additional heat is generated in the non-lasing situation (i.e. for conditions of higher excitation density). The increased heat load has a number of undesirable consequences, such as spherical aberration in the thermally-induced lens with consequent degradation in beam quality and higher resonator losses. Ultimately with sufficient heat load rod fracture will occur. With that effect being particularly pronounced under non-lasing conditions, Q-switched operation and operation as an amplifier will be especially susceptible. So a good understanding of the processes underlying this deterioration in performance is required if optimal performance is to be achieved from diode-pumped Nd^{3+}:$LiYF_4$ lasers.

Recent research indicates that this deterioration arises from interionic processes involving ions in the upper laser level as well as reabsorption of laser photons from several levels [12-21]. A rate parameter for the interionic upconversion process in Nd^{3+}:$LiYF_4$ was recently published by Guyot et al. [19]. The influence of ground-state bleaching and its implication for reduced pump-absorption efficiencies has as yet not been considered.

In this paper we report investigations of the combined effects of ground-state bleaching, interionic upconversion, and lifetime quenching in the Nd^{3+}:$LiYF_4$ system under intense end-pumping conditions. The experimental data are found to be in good agreement with a finite-element rate-equation calculation, which takes into account the spatial variation of the relevant processes. The spatially resolved influence of upconversion on the storage time of the system is calculated in the simulation. Approximate analytical expressions for the dependence of ground-state bleaching, excitation, and storage time on pump parameters and dopant concentration are derived.

2. Interionic Processes

Several authors [13,21-24] have measured Stark-level energies of various multiplet levels in Nd^{3+}:$LiYF_4$. A selection from their data is summarized in Table 1, from which the possible spectral overlap of emission and absorption lines which may lead to the occurrence of interionic processes can be identified. Since only the $^4F_{3/2}$ level has a long lifetime, only interionic processes which involve this level are of significant importance. The partner ion in the process can also be in this level, leading to upconversion processes, or be in the ground state, leading to cross-relaxation processes.

The processes which have a direct or indirect (phonon-assisted) spectral overlap between emission and absorption are presented in Table 2. Four upconversion processes UC_1-UC_4 are identified for Nd^{3+}:$LiYF_4$, which coincide with those suggested for Nd^{3+}-doped glasses [17]. For the three processes UC_1-UC_3, see Fig. 1, a direct overlap of the short-wavelength (high-energy) side of emission with absorption is present in $LiYF_4$, which suggests that these processes may have a significant influence. The influence of process UC_4 is probably negligible, because it has

only a phonon-assisted overlap. The dependence of the rates of these processes on the excitation of the $^4F_{3/2}$ level is quadratic.

Two cross-relaxation processes have been suggested [18]: Process CR_1 (see Table 2) exhibits a direct overlap of the short-wavelength side of emission with the long-wavelength side of absorption, again indicating the possibility of a significant influence. The dependence of this process on absorbed pump intensity is less than linear, because the population of the ground state, which is one of its initial levels, decreases with pump intensity. The energy mismatch of emission and absorption is relatively large for processes CR_2 and CR_3, making these processes less likely to occur. In $LiYF_4$ it requires the emission of two phonons. Processes CR_2 and CR_3 lead to identical results in the population mechanisms of the system. Thus, they cannot be distinguished by spectroscopic means.

The interionic processes which may be of importance (UC_1-UC_3, CR_1) are investigated here with respect to their spectral overlap and its dependence on host temperature between 250 and 500 K. Any temperature dependence of these interionic processes could be relevant to laser operation, because substantial additional heat is created by cascaded multiphonon relaxation following each upconversion process, leading to significant increase in temperature, which, in return, may further stimulate upconversion. A rapid degradation in laser performance with increase in temperature can then result from unfavorable temperature dependence of various parameters, such as the thermal conductivity, dependence of refractive index on temperature etc.

As in Ref. [19], we integrate the overlap of calculated emission and absorption spectra. The positions of the energy levels of Table 1 are used and the simplifying assumptions are made that all Stark transitions have the same transition strengths and are of Lorentzian shape with a temperature-independent line width (FWHM) of 30 cm^{-1} (this being a typical observed value). The temperature dependence of the overlap integral arises due to the Boltzmann distribution of the population densities in the Stark sub-levels of the emitting and absorbing levels.

The three upconversion processes UC_1-UC_3 are all found to be rather insensitive to temperature changes, the overlap typically changing less than 5 % from 250-500 K. This results from the fact that both the emission and absorption processes originate from a level ($^4F_{3/2}$) with two Stark sub-levels which have only a small energy gap and thus have comparable population at

room temperature and which both contribute to transitions in the overlap regions of the upconversion processes. The cross-relaxation process CR_1 is found to depend strongly on temperature, because its overlap region includes transitions originating from the high-lying Stark levels of the ground state, but the overlap remains small compared to those of the upconversion processes even at room temperature. A cubic dependence of non-radiative ion-ion interaction on temperature was found for Nd^{3+}-doped fluoride glasses [15] at temperatures below 100 K.

Calculated values for the Lorentzian overlap integrals L at room temperature (in arbitrary units) are: $L(UC_1) = 0.14$, $L(UC_2) = 0.19$, $L(UC_3) = 0.29$, $L(CR_1) = 0.03$. According to Dexter [25], the interaction probability c_{DA} is proportional to this overlap integral as well as to the radiative decay rate A of the emission process, i.e. $c_{DA} \propto L\,A$. With the radiative decay rates calculated from Judd-Ofelt theory [26], $A_{43} = 11\ s^{-1}$, $A_{42} = 221\ s^{-1}$, $A_{41} = 1006\ s^{-1}$, this yields $c_{DA}(UC_1) / c_{DA}(UC_2) / c_{DA}(UC_3) / c_{DA}(CR_1) \propto 1.5\ s^{-1} / 42\ s^{-1} / 292\ s^{-1} / 0.3\ s^{-1}$. This identifies processes UC_3 and UC_2 as the most important interionic processes in Nd^{3+}:$LiYF_4$ over the investigated temperature range from 250-500 K.

Taking further into account that c_{DA} is proportional to the integral absorption cross-section and using the Judd-Ofelt parameters of Ref. [19], we find $c_{DA}(UC_2) / c_{DA}(UC_3) \propto 1.1\text{x}10^{-19}\ cm^2s^{-1} / 6.2\text{x}10^{-19}\ cm^2s^{-1}$. In Ref. [19] a larger ratio between the overlap of UC_3 and UC_2 was calculated from measured spectra of fluorescence and excited-state absorption at room temperature. This disagreement possibly originates in our oversimplification of assuming equal Stark-transition strengths. Nevertheless, these two processes seem to be the most important, with UC_3 being stronger than UC_2, and both having little temperature dependence in the investigated temperature range.

3. Experimental

The set-up for the determination of absorbed pump power and fluorescence signal is shown in Fig. 2. A Ti:sapphire laser with pump wavelength tuned to the Nd^{3+}:$LiYF_4$ absorption peak at $\lambda_p = 797$ nm and a measured beam-quality factor of $M^2 = 1.20$ is used as a pump source. A pump power of $P_{in} = 305$ mW incident on the focusing lens is available, of which a fraction of $\eta_{in} =$

94 % is transmitted into the sample. Different pump powers are selected using a variable attenuator. The pump beam is focused into the crystal with a lens of focal length f = 50 mm. The measured beam-waist radius is w_{p0} = 30 μm.

A Nd^{3+}:$LiYF_4$ crystal of length ℓ = 6 mm, refractive index n_r = 1.46, and a Nd^{3+} concentration of N_d = 1.59 x 10^{20} cm^{-3} (= 1.15 at.% in $LiYF_4$) is used for the spectroscopic investigation. The front and back surfaces are antireflection coated at the pump wavelength. The pump radiation is absorbed on the ground-state transition $^4I_{9/2} \rightarrow {}^4F_{5/2}$, see Fig. 1. The transmitted pump power is measured with a detector.

The absorbed pump power versus incident pump power is displayed in Fig. 3a. The dashed line extrapolates the fraction of pump power absorbed at low input-power levels and the amount of ground-state bleaching is therefore indicated by the deviation of the measured data (squares) from the dashed line. The influence of bleaching, which, in this measurement, is averaged over the whole sample length and over the gaussian shape of the pump beam, leads to a decrease in absorption of 10 % at our highest pump power. The sample was placed in the set-up with arbitrary axis orientation relative to the polarization of the pump light. The relevant effective absorption cross-section for the arrangement, which was maintained throughout the experiment, was calculated from the data at low pump power where ground-state bleaching is not present. The value is σ_p = 1.9 x 10^{-20} cm^2.

The largest cross-sections for excited-state absorption in the spectral region of the pump wavelength have values [19] of less than 0.02 of the strong cross-section for ground-state absorption at 797 nm, and since the excitation of the sample does not exceed 18 % (see later in Section V), it follows that pump excited-state absorption contributes certainly less than 1 % to the total observed absorption at 797 nm and hence can be neglected.

The sample is excited on a pump-beam path which is close to one side surface of the sample in order to minimize any fluorescence reabsorption. The fluorescence signal on the multiplet transition $^4F_{3/2} \rightarrow {}^4I_{11/2}$ at 1.03-1.09 μm is collected from that side of the crystal with an objective (20x), coupled into a fiber, and analyzed by an ANDO spectrum analyzer. The objective is positioned in such a way that the fluorescence from a small area of approximately 50 μm radius within the first 10 % of the crystal length is detected.

If the fluorescence signal is observed during the process of reducing the distance of the focusing lens from the sample, with decreasing pump spot-size at the detected area, first the fluorescence signal increases, as a larger fraction of the transverse extent of the pump is contained within the detected area. As the pump spot within the detected area further decreases below ~ 50 μm radius, the fluorescence signal begins to decrease, as the entire pump-beam width is contained within the detected area, but ground-state bleaching increases and upconversion processes compete more successfully with radiative decay. The minimum of the fluorescence signal corresponds to the pump focus being located at the detected region of the crystal. Further reduction of the distance between focal lens and crystal reverses the observed behavior of the fluorescence signal.

The measurement is performed with the focus in the detected area. The signals of the two highest fluorescence peaks at 1.047 μm and 1.053 μm are added for the determination of the signal intensity versus pump power. Fig. 3b reveals a significant saturation of the investigated fluorescence (squares) with a deviation at highest pump power of more than 50 % from the extrapolated data at low pump power (dashed line).

4. Rate Equations

In a computer simulation involving the relevant levels (ground state and eight excited states, see Fig. 1) and processes (pump power and configuration, ground-state absorption and depletion, all lifetimes and branching ratios, three interionic processes, and the crystal data), time- and space-dependent rate equations describing the Nd^{3+}:$LiYF_4$ system are solved numerically. The population dynamics are calculated and the amounts of ground-state bleaching, upconversion, and lifetime quenching are investigated.

The Nd^{3+}:$LiYF_4$ lifetimes τ_i represent the intrinsic lifetimes of the system at low dopant concentration and include radiative as well as multiphonon relaxations. The $^4F_{3/2}$ lifetime of τ_4 = 520 μs is taken from Ref. [27] and the $^4I_{13/2}$ lifetime of $\tau_1 \approx 20$ ns was measured in Refs. [4,5]. The lifetimes of the $^2G(1)_{9/2}$, $^4G_{7/2}$, $^4G_{5/2}$, $^4F_{5/2}$, $^4I_{15/2}$, and $^4I_{13/2}$ levels are in the order of the $^4I_{13/2}$ lifetime. Since no data are available in literature, they are assumed as τ_i = 50 ns. It is found

that these lifetimes are not crucial for the calculation as long as they are short enough to ensure that no significant excitation is accumulated in the corresponding levels. In the present case the calculated excitations of these levels are in the order of $<10^{-6}$ of the ground-state population.

Judd-Ofelt data [26] of Nd^{3+}:$LiYF_4$ for the radiative rates from the $^4F_{3/2}$ level are: A_{40} = 619 s^{-1}, A_{41} = 1006 s^{-1}, A_{42} = 221 s^{-1}, A_{43} = 11 s^{-1}. Assuming a fluorescence lifetime of 520 μs, this leads to a nonradiative rate of A_{nr} = 66 s^{-1} into the next lower-lying level. The branching ratios β_{4j} from the $^4F_{3/2}$ level (including radiative and multiphonon decay) are calculated from these data in the same way as in Ref. [28]: β_{40} = 0.322, β_{41} = 0.523, β_{42} = 0.115, and β_{43} = 0.040.

All other levels are assumed to decay completely via strong multiphonon relaxation [1-5] into their next lower-lying levels. Visible fluorescences from the high-lying excited levels $^4G_{5/2}$, $^4G_{7/2}$, and $^2G(1)_{9/2}$ are negligible. These channels contribute with branching ratios of probably less than 0.001 to the de-excitation rates of the high-lying levels. A few extremely high-lying levels possess lifetimes in the μs range and may decay predominantly radiatively [29,30], but these levels are not populated by the dominant upconversion processes investigated here.

The three upconversion processes UC_1-UC_3 of Table 2 and Fig. 1 are considered in the simulation. The measured parameter [19] of combined upconversion is $W = 1.7\text{x}10^{-16}$ cm^3/s. Considering the investigations of Section II, we assume that the individual processes have parameters $W_1 = 0.01\text{x}10^{-16}$ cm^3/s, $W_2 = 0.26\text{x}10^{-16}$ cm^3/s, and $W_3 = 1.43\text{x}10^{-16}$ cm^3/s. Different values would lead to similar results in the calculation, because all terminating levels of the upconversion processes exhibit fast multiphonon decays into the $^4F_{3/2}$ and $^4I_{9/2}$ levels, respectively. The cross-relaxation process CR_1 discussed in Section II is neglected, because its spectral overlap is comparatively small.

The parameters of the experiment presented in Section III are taken into account. Let z and r be the variables of longitudinal and radial coordinate within the crystal, respectively. They represent the discrete longitudinal elements z = 1 to n covering the crystal length ℓ as well as the discrete radial cylinder elements r = 1 to m covering twice the maximum pumped radius $w_p(z = n)$ at the position of the last longitudinal element at the crystal back surface. A finite-element resolution of n = 8 and m = 15 is chosen for the calculation. With $\boldsymbol{r} = (r, z)$, the space vector,

$r_1(r)$ and $r_2(r)$, the inner and outer radii of the radial element r, and $\Delta\ell(z)$, the length of the longitudinal element z, the rate equations for the population densities $N_i(\mathbf{r})$ read:

$$dN_8(\mathbf{r})/dt = W_3 N_4^2(\mathbf{r}) - \tau_8^{-1} N_8(\mathbf{r}) \quad (1)$$

$$dN_7(\mathbf{r})/dt = W_2 N_4^2(\mathbf{r}) + \tau_8^{-1} N_8(\mathbf{r}) - \tau_7^{-1} N_7(\mathbf{r}) \quad (2)$$

$$dN_6(\mathbf{r})/dt = W_1 N_4^2(\mathbf{r}) + \tau_7^{-1} N_7(\mathbf{r}) - \tau_6^{-1} N_6(\mathbf{r}) \quad (3)$$

$$dN_5(\mathbf{r})/dt = R_{05}(\mathbf{r}) + \tau_6^{-1} N_6(\mathbf{r}) - \tau_5^{-1} N_5(\mathbf{r}) \quad (4)$$

$$dN_4(\mathbf{r})/dt = \tau_5^{-1} N_5(\mathbf{r}) - \tau_4^{-1} N_4(\mathbf{r}) - 2\left[W_1 + W_2 + W_3\right] N_4^2(\mathbf{r}) \quad (5)$$

$$dN_3(\mathbf{r})/dt = \beta_{43} \tau_4^{-1} N_4(\mathbf{r}) - \tau_3^{-1} N_3(\mathbf{r}) + W_1 N_4^2(\mathbf{r}) \quad (6)$$

$$dN_2(\mathbf{r})/dt = \beta_{42} \tau_4^{-1} N_4(\mathbf{r}) + \tau_3^{-1} N_3(\mathbf{r}) - \tau_2^{-1} N_2(\mathbf{r}) + W_2 N_4^2(\mathbf{r}) \quad (7)$$

$$dN_1(\mathbf{r})/dt = \beta_{41} \tau_4^{-1} N_4(\mathbf{r}) + \tau_2^{-1} N_2(\mathbf{r}) - \tau_1^{-1} N_1(\mathbf{r}) + W_3 N_4^2(\mathbf{r}) \quad (8)$$

$$dN_0(\mathbf{r})/dt = - R_{05}(\mathbf{r}) + \beta_{40} \tau_4^{-1} N_4(\mathbf{r}) + \tau_1^{-1} N_1(\mathbf{r}). \quad (9)$$

The absorption coefficient is

$$\alpha(\mathbf{r}) = \sigma_p N_0(\mathbf{r}). \quad (10)$$

The pump-beam radius (with its waist w_{p0} at the crystal front surface $z = 0$) is given by

$$w_p(z)^2 = w_{p0}^2 + \left(\frac{z M^2 \lambda_p}{\pi n_r w_{p0}} \right)^2, \quad (11)$$

The fraction $\rho_p(\boldsymbol{r})$ of the power of the gaussian pump beam [31] contained in the cylinder at $\boldsymbol{r}$ compared with the total pump power in the longitudinal element z is

$$\rho_p(\mathbf{r}) = 2 / [\pi w_p(z)^2] \int_{r_1(r)}^{r_2(r)} \exp[-2 r''^2 / w_p(z)^2] \, 2 \pi r'' \, dr''$$

$$= \exp[-2 r_1(r)^2 / w_p(z)^2] - \exp[-2 r_2(r)^2 / w_p(z)^2]. \qquad (12)$$

The power $P_l(z)$ which is launched into the longitudinal element z is calculated as

$$P_l(z) = \eta_{in} P_{in} \prod_{z'=1}^{z-1} \left\{ \sum_{r'=1}^{m} [\rho_p(\mathbf{r}') \exp(\Delta\ell(z') \alpha(\mathbf{r}'))] \right\}, \qquad (13)$$

It is an implication of eqs. (12) and (13) that after absorption of the pump power in each longitudinal element a gaussian pump shape is maintained, i.e., a possible degradation of the gaussian pump shape due to ground-state bleaching and, therefore, radially non-uniform absorption is neglected. With eqs. (10)-(13), the equation for the pump rate $R_{05}(\boldsymbol{r})$ per unit volume from the ground state into the $^4F_{5/2}$ level reads:

$$R_{05}(\mathbf{r}) = \left\{ 1 - \exp[\Delta\ell(z) \alpha(\mathbf{r})] \right\} \frac{\lambda_p}{hc} \frac{P_l(z) \rho_p(\mathbf{r})}{\Delta\ell(z) \pi \left[r_2(r)^2 - r_1(r)^2 \right]} . \qquad (14)$$

h and c denote Planck's constant and the vacuum speed of light, respectively. The rate equations are solved in a Runge-Kutta calculation of fourth order.

5. Numerical Results

The experimental situation described in Section III is modeled with the rate equations of Section IV taking into consideration the three upconversion processes discussed in Section II (see Fig. 1). In Fig. 3a the amount of absorbed pump power versus incident power derived from the

simulation (solid line) is compared with the experimental data (squares). For Fig. 3b, the calculated fluorescence signals on the transition $^4F_{3/2} \rightarrow {}^4I_{11/2}$ at 1.03-1.09 μm from all spatial elements within the first 10 % of the crystal length are summed (solid line). The derived dependence on pump power is calibrated to the arbitrary units of the measured signal (squares) in Fig. 3b in such way that the straight-line extrapolation (dashed line) from the low-power behavior, for experimental and calculated behavior, coincide.

Since ground-state bleaching and especially fluorescence saturation depend strongly on the lifetime quenching due to upconversion, the good agreement of experiment and calculation in Figs. 3a and b is a confirmation of the upconversion parameter of 1.7×10^{-16} cm^3/s measured by Guyot et al. [19]. This value is a factor of two to seven times higher than in Nd^{3+}-doped glasses [17]. Variation of the upconversion parameter used in the simulation and comparison with the experimental data reveals that our experiment confirms the parameter with an error margin of approximately ±30 %. This result is of importance, because the measurement method used here is different from that of Ref. [19]. In fact we use this result in a further publication [32] to calculate upconversion-dependent heat generation and thermal lensing in Nd^{3+}:$LiYF_4$ and compare the calculated results with our measurements [11]. We use it here for a spatially resolved calculation of ground-state bleaching and storage time from the rate equations of Section IV.

The experimental situation of Section III at highest pump power (P_{in} = 305 mW) is chosen for this calculation. The resulting spatially resolved ground-state bleaching is shown in Fig. 4a. At the point of highest pump intensity (the center of the gaussian pump beam at the crystal front surface) the ground-state bleaching reaches 18 %. Since the $^4F_{3/2}$ level is the only metastable and significantly populated level, its excitation is equal to the amount of ground-state bleaching.

The concept of "lifetime" or "storage time" is no longer straightforward when non-linear processes are involved in the de-excitation, as in the case of the upconversion processes from the $^4F_{3/2}$ level. The fluorescence decay is not exponential and a lifetime cannot be associated with this decay. One can define a 1/e-decay time, i.e. the time for the excited-state population to decay to 1/e from its initial value. However, the contribution to the decay rate resulting from upconversion decreases significantly over the 1/e-decay time. A more appropriate definition of

the storage time under cw excitation is the inverse depletion rate of the $^4F_{3/2}$ level in the steady state. It can be measured as the inverse fluorescence decay rate at the moment the pump is switched off. This definition will be used in the following.

The spatially resolved storage time as calculated from our rate-equation model is shown in Fig. 4b. At the point of highest pump intensity, the storage time drops from 520 to 145 μs (for comparison: the 1/e-decay time at this point is 208 μs). Experimental detection of the fluorescence decay from the side surface will lead to an average over the different radial decay rates of Fig. 4b. Integration of the fluorescent emission over all spatial elements within the first 10 % of the crystal length yields a storage time of 186 μs. The averaged absorbed pump density in the corresponding volume is 25 W/mm^3. This lifetime quenching, in combination with ground-state bleaching (Fig. 3a), leads to the fluorescence saturation measured and calculated in Fig. 3b. Ground-state bleaching is decreased by lifetime quenching. Without upconversion, the amount of ground-state bleaching would be much larger (e.g., 43 % at the point of highest pump intensity).

Fig. 4 may serve as an example to demonstrate that under non-lasing or Q-switched conditions high excitation of the upper laser level and consequent upconversion losses will significantly affect the storage time of the system. The Ti:sapphire intensity incident on the crystal is 10 kW / cm^2 in our experiment. Such an intensity can easily be provided by beam-shaped high-power laser-diode bars [33] as well. Hence, the results presented here are also applicable to high-power diode-pumped Nd^{3+}:$LiYF_4$ lasers.

6. Analytical Treatment

The rate-equation scheme of Section IV can be simplified by considering that 1) levels 1-3 and levels 5-8 exhibit a fast decay to the ground state and level 4, respectively, 2) the different upconversion processes lead to similar results concerning the populations of levels 0 and 4 and can thus be expressed by a single parameter $W = 1.7\text{x}10^{-16}$ cm^3/s, and 3) the effect is for only one excitation to be removed from level 4 by each upconversion process, because the excitation of its high-lying terminating state will decay and return to its initial level. We further assume 4) a

small element of length x and area A, into which a pump power P_l or pump intensity I_l is launched. The above considerations lead to the reduction of the rate-equation system (1)-(9) to two rate equations,

$$dN_4/dt = R_{04} - \tau_4^{-1} N_4 - W N_4^2 \tag{15}$$

$$N_0 = N_d - N_4, \tag{16}$$

for the $^4F_{3/2}$ level and the ground state. Expansion of the pump rate of eq. (14) into a Taylor series yields

$$R_{04} = [1 - \exp(x \sigma_p N_0)] \frac{\lambda_p}{hc} \frac{P_l}{x A}$$

$$\approx \sigma_p \frac{\lambda_p}{hc} I_l N_0. \tag{17}$$

Introducing the abbreviation

$$C = \sigma_p \frac{\lambda_p}{hc} I_l, \tag{18}$$

combination of eqs. (15)-(17) provides the excitation (and ground-state bleaching):

$$N_4 = \{ - (\tau_4^{-1} + C) + [(\tau_4^{-1} + C)^2 + 4 W C N_d]^{0.5} \} / (2 W). \tag{19}$$

The storage time including upconversion quenching is then given by

$$\tau_{eff}^{-1} = \tau_4^{-1} + W N_4 \tag{20}$$

which is the sum of the depletion rates in eq. (15).

Equation (19) represents an analytical expression for the dependence of ground-state bleaching and excitation of the $^4F_{3/2}$ level on pump intensity, absorption cross-section, and dopant concentration under the consideration of interionic upconversion. From eq. (20) the averaged or, in successive longitudinal steps, the spatially resolved lifetime quenching of any specific device can be calculated. Using the parameters of Sections III and IV and assuming a uniform pump intensity within a cylinder of radius w_{p0} = 30 µm as well as $P_l = \eta_{in} P_{in}$, we derive a storage time of 187 µs. This value is in good agreement with the result of 186 µs, which was obtained in Section V from integrating the spatially resolved solution of the full rate-equation system over the first 10 % of the crystal length.

This result shows that under non-lasing conditions the radial approximation of a gaussian beam of waist w_{p0} by a uniform cylindrical beam of radius w_{p0} can give a good approximation despite the fact that the upconversion process involved is non-linear. This also explains why our spatially resolved approach is able to confirm a parameter that was in fact derived by solving equations that were not spatially resolved [19].

7. Conclusions

Ground-state bleaching and fluorescence saturation were measured in Nd^{3+}:$LiYF_4$ under strong Ti:sapphire excitation. The experimental data were found to be in good agreement with measured data obtained from a finite-element rate-equation calculation. The published value of the upconversion parameter of 1.7×10^{-16} cm^3/s has been confirmed with good accuracy. The temperature dependence of the involved interionic processes is probably small over a wide temperature range. A spatially resolved ground-state bleaching of up to 18 % and a quenching of the storage time from 520 down to 145 µs at the point of highest pump irradiance were calculated in the simulation for a gaussian pump of 305 mW focused down to a radius of 30 µm. The radially integrated storage time is 186 µs for an absorbed pump density of 25 W/mm^3. Approximate analytical expressions for the dependence of ground-state bleaching, excitation density, and storage time on the parameters of pump intensity, absorption cross-section, and

dopant concentration under the influence of interionic upconversion were derived and the validity of the analytical approximation was confirmed.

The presence of the upconversion processes is shown to have a significant effect on the decay of excitation from the $^4F_{3/2}$ level under pumping conditions not dissimilar from those used in actual end-pumped laser devices. A consequence of this additional decay rate is that significant extra heat loading can occur in Nd^{3+}:$LiYF_4$ when high excitation density is involved, as for example in Q-switching or in an amplifier configuration. Further experiments have quantitatively confirmed the strong contribution to thermal lensing made by the upconversion processes, and, now that a quantitative model is available, appropriate design strategies can be derived for significant power scaling of diode-end-pumped Nd^{3+}:$LiYF_4$ lasers.

Acknowledgments

The authors gratefully acknowledge support from their colleagues at the Optoelectronics Research Centre, University of Southampton, United Kingdom. We thank Charles Haythornthwaite and Jason Hector for technical assistance, and Rüdiger Paschotta for helpful discussions concerning the implementation of the computer program. Parts of the source code were developed during an earlier work at the Institute of Applied Physics, University of Bern, Switzerland. M. Pollnau is supported by a fellowship from the European Union within the "Human Capital and Mobility Programme". P. J. Hardman acknowledges the support of Lumonics, Ltd., in the form of a Cooperative Award in Science and Engineering studentship.

References

[1] T. T. Basiev, A. Y. Dergachev, Y. V. Orlovskii, and A. M. Prokhorov, J. Lumin. **53**, 19-23 (1992).

[2] Y. V. Orlovskii, R. J. Reeves, R. C. Powell, T. T. Basiev, and K. K. Pukhov, Phys. Rev. B **49**, 3821-3830 (1994).

[3] Y. V. Orlovskii, T. T. Basiev, I. N. Vorob'ev, V. V. Osiko, A. G. Papashvili, and A. M. Prokhorov, Laser Phys. **6**, 448-455 (1996).

[4] J. D. Zuegel and W. Seka, IEEE J. Quantum Electron. **31**, 1742-1746 (1995).

[5] C. Bibeau, S. A. Payne, and H. T. Powell, J. Opt. Soc. Am. B **12**, 1981-1992 (1995).

[6] W. Seelert, H. P. Kortz, and W. M. Yen, "Excited state absorption and F lifetime shortening in diode pumped Nd:YLF Q-switch lasers", in Proceedings on Advanced Solis-Stae Lasers, Vol. **13**, ed. L. L. Chase and A. A. Pinto (Optical Society of America, Washington, DC, 1992), pp. 209-211.

[7] R. Beach, P. Reichert, W. Benett, B. Freitas, S. Mitchell, A. Velsko, J. Darwin, and R. Solarz, Opt. Lett. **18**, 1326-1328 (1993).

[8] H. Vanherzeele, Opt. Lett. **13**, 369-371 (1988).

[9] G. Cerullo, S. de Silvestri, and V. Magni, Opt. Commun. **93**, 77-81 (1992).

[10] C. Pfistner, R. Weber, H. P. Weber, S. Merazzi, and R. Gruber, IEEE J. Quantum Electron. **30**, 1605-1615 (1994).

[11] P. J. Hardman, W. A. Clarkson, M. Pollnau, and D. C. Hanna, to be published.

[12] T. Y. Fan, G. J. Dixon, and R. L. Byer, Opt. Lett. **11**, 204-206 (1986).

[13] M. Malinowski, B. Jacquier, M. Bouazaoui, M. F. Joubert, and C. Linares, Phys. Rev. B **41**, 31-40 (1990).

[14] A. T. Stanley, E. A. Harris, T. M. Searle, and J. M. Parker, J. Non-Crystalline Solids **161**, 235-240 (1993).

[15] R. Balda, J. Fernández, A. Mendioroz, J. L. Adam, and B. Boulard, J. Phys.: Condens. Matter **6**, 913-924 (1994).

[16] A. d. Novo-Gradac, W. M. Dennis, A. J. Silversmith, S. M. Jacobsen, and W. M. Yen, J. Lumin. **60+61**, 695-698 (1994).

[17] S. A. Payne, G. D. Wilke, L. K. Smith, and W. F. Krupke, Opt. Commun. **111**, 263-268 (1994).

[18] B. Viana, A. M. Lejus, D. Saber, N. Duxin, and D. Vivien, Opt. Materials **3**, 307-316 (1994).

[19] Y. Guyot, H. Manaa, J. Y. Rivoire, R. Moncorgé, N. Garnier, E. Descroix, M. Bon, and P. Laporte, Phys. Rev. B **51**, 784-799 (1995).

[20] T. Chuang and H. R. Verdún, IEEE J. Quantum Electron. **32**, 79-91 (1996).

[21] Y. Guyot and R. Moncorge, J. Appl. Phys. 73, 8526-8530 (1993).

[22] A. A. S. da Gama, G. F. de Sá, P. Porcher, and P. Caro, J. Chem. Phys. **75**, 2583-2587 (1981).

[23] A. L. Harmer, A. Linz, and D. R. Gabbe, J. Phys. Chem. Solids **30**, 1483-1491 (1969).

[24] F. G. Anderson, H. Weidner, P. L. Summers, and R. E. Peale, J. Lumin. **62**, 77-84 (1994).

[25] D. L. Dexter, J. Chem. Phys. **21**, 836-850 (1953).

[26] C. Li, Y. Guyot, C. Linarès, R. Moncorgé, and M. F. Joubert, "Radiative transition probabilities of trivalent rare-earth ions in $LiYF_4$", in Advanced Solid-State Lasers and Compact Blue-Green Lasers Technical Digest, 1993 (Optical Society of America, Washington, D.C., 1993), Vol. **2**, pp.423-425.

[27] J. R. Ryan and R. Beach, J. Opt. Soc. Am. B **9**, 1883-1887 (1992).

[28] M. Pollnau, Th. Graf, J. E. Balmer, W. Lüthy, and H. P. Weber, Phys. Rev. A **49**, 3990-3996 (1994).

[29] B. Jacquier, M. Malinowski, M. F. Joubert, and R. M. Macfarlane, J. Lumin **45**, 357-359 (1990).

[30] M. F. Joubert, B. Jacquier, C. Linares, and R. M. Macfarlane, J. Lumin. **53**, 477-482 (1992).

[31] W. P. Risk, J. Opt. Soc. Am. B **5**, 1412-1423 (1988).

[32] M. Pollnau, P. J. Hardman, W. A. Clarkson, and D. C. Hanna, to be published.

[33] W. A. Clarkson and D. C. Hanna, Opt. Lett. **21**, 375-377 (1996).

Table 1. Stark-level energies [cm^{-1}] of various multiplet levels of Nd^{3+}:$LiYF_4$. The second column refers to the theoretical number of Stark levels. Data are summarized from the given References. Italic style denotes a calculated value.

Level	St	No. 1	No. 2	No. 3	No. 4	No. 5	No. 6	No. 7	No. 8	Ref.
$^2P_{1/2}$	1	23420								[22]
$^2G(1)_{9/2}$	5	*21016*	21066	21079	21084	21119				[22]
$^4G_{7/2}$	4	19055	19071	19172	19201					[21]
$^4G_{5/2}$	3	17154	17265	17293						[13]
$^4F_{3/2}$	2	11538	11597							[23]
$^4I_{15/2}$	8	5848.5	5909.5	5944.9	6031.5	6312.6	6346.1	6390.0	6431.8	[24]
$^4I_{13/2}$	7	3947.2	3975.9	3993.9	4023.5	4204.4	4214.3	4239.5		[24]
$^4I_{11/2}$	6	1997.1	2040.1	2042.4	2077.0	2226.8	2261.0			[24]
$^4I_{9/2}$	5	0.0	132.1	182.5	247.2	526.6				[24]

Table 2. Overlap of emission and absorption of possible interionic processes. Given are the emission process, its energy width ΔE_{em}, the absorption process that leads to direct or indirect overlap of emission and absorption, and its energy width ΔE_{abs}. Processes CR_2 and CR_3 lead to identical results in the population mechanisms of the system and cannot be distinguished by spectroscopic means.

Process	Emission	ΔE_{em} [cm^{-1}]	Absorption	ΔE_{abs} [cm^{-1}]
UC_1	$^4F_{3/2} \rightarrow {}^4I_{15/2}$	5106-5749	$^4F_{3/2} \rightarrow {}^4G_{5/2}$	5557-5755
UC_2	$^4F_{3/2} \rightarrow {}^4I_{13/2}$	7299-7650	$^4F_{3/2} \rightarrow {}^4G_{7/2}$	7458-7663
UC_3	$^4F_{3/2} \rightarrow {}^4I_{11/2}$	9277-9600	$^4F_{3/2} \rightarrow {}^2G(1)_{9/2}$	9468-9578
UC_4	$^4F_{3/2} \rightarrow {}^4I_{9/2}$	11011-11597	$^4F_{3/2} \rightarrow {}^2P_{1/2}$	11822, 11879
CR_1	$^4F_{3/2} \rightarrow {}^4I_{15/2}$	5106-5749	$^4I_{9/2} \rightarrow {}^4I_{15/2}$	5322-6432
CR_2	$^4F_{3/2} \rightarrow {}^4I_{15/2}$	5106-5749	$^4I_{9/2} \rightarrow {}^4I_{13/2}$	3421-4240
CR_3	$^4F_{3/2} \rightarrow {}^4I_{13/2}$	7299-7650	$^4I_{9/2} \rightarrow {}^4I_{15/2}$	5322-6432

Figure Captions

Fig. 1. Energy-level scheme of Nd^{3+}:$LiYF_4$. Energy levels which are denoted by their spectroscopic terms are included in the computer model. Processes that are relevant for the population of the $^4F_{3/2}$ level: pump absorption with a rate R_{05}, fluorescent transitions from the $^4F_{3/2}$ level, upconversion processes UC_1, UC_2, and UC_3 from the $^4F_{3/2}$ level. Cascaded multiphonon de-excitation following each process is indicated by a dashed line.

Fig. 2. Experimental set-up for the measurement of pump absorption and fluorescence intensity. The pump excitation occurs close to the surface from where the fluorescence is collected. The fluorescence is detected within the first 10 % of the crystal length.

Fig. 3. a) Absorbed pump power versus incident pump power: experimental data (squares), calculation (solid line), and deviation from extrapolation (dashed line) of the low-power data owing to ground-state bleaching. b) fluorescence intensity versus incident pump power: experimental data (squares), calculation (solid line), and deviation from extrapolation (dashed line) owing to ground-state bleaching and upconversion.

Fig. 4. Calculated spatial resolution of a) ground-state population and b) $^4F_{3/2}$ fluorescence lifetime versus the crystal length of 6 mm and the $1/e^2$ gaussian pump radius at the crystal front surface of 30 μm. The front-left corners of the figures represent the center of the gaussian pump beam at the crystal front surface. The pump power is 305 mW, which corresponds to the highest power available in the experiment.

Figure 1 **M. Pollnau et al.** **Opt. Commun.**

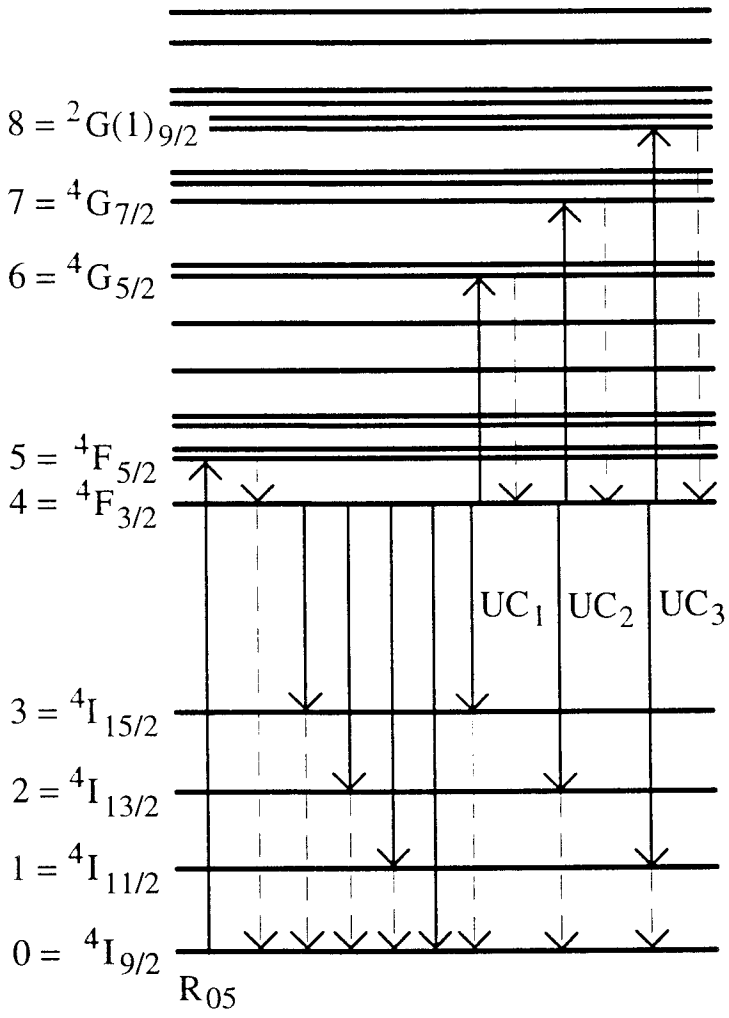

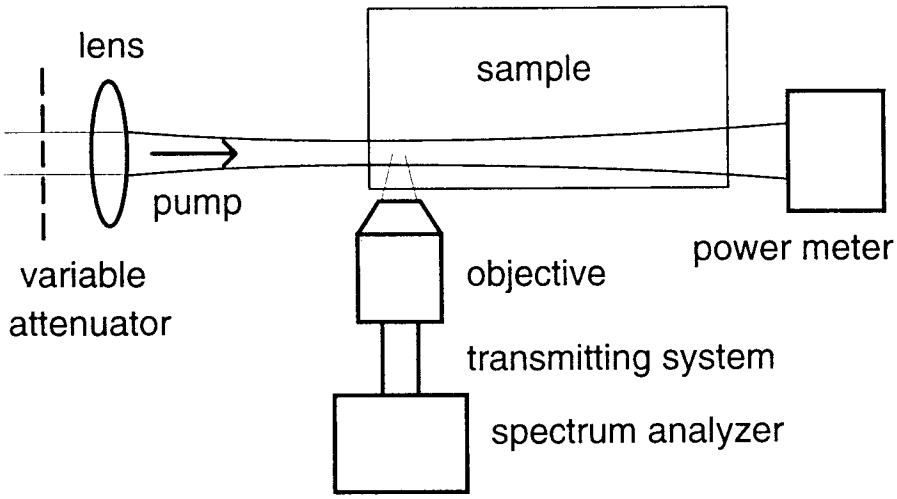
lens
sample
pump
variable
attenuator
objective
power meter
transmitting system
spectrum analyzer

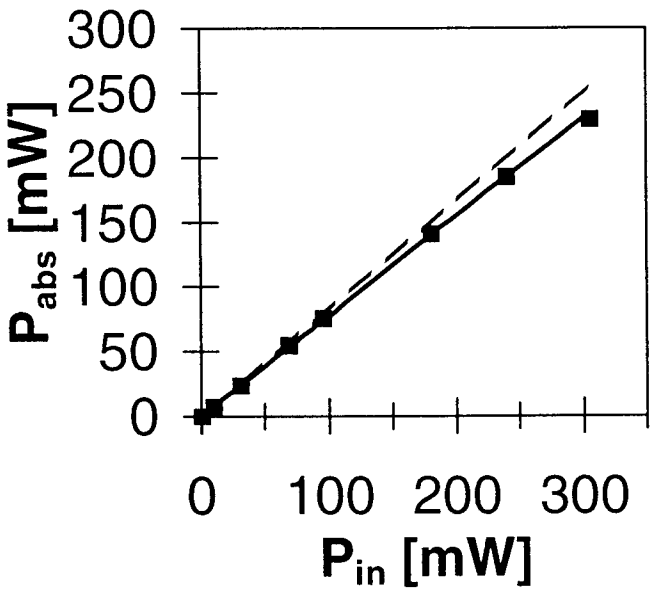
300
250
200
150
100
50
0
P_{abs} [mW]
0
100
200
300
P_{in} [mW]

Figure 3 b) M. Pollnau et al. Opt. Commun.

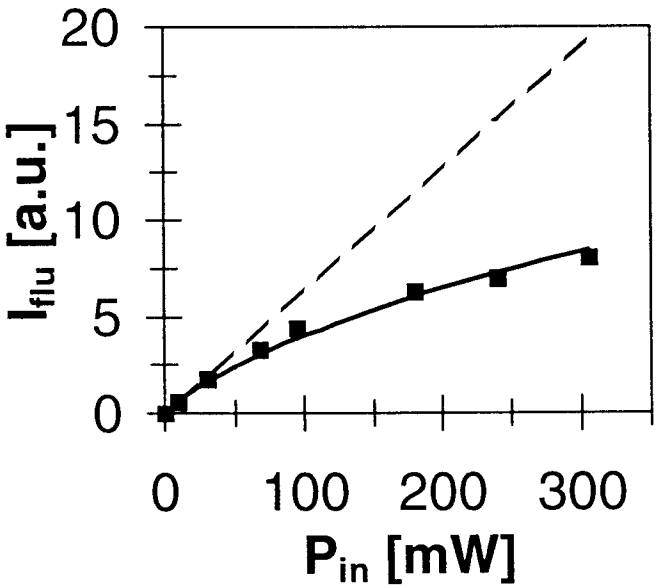

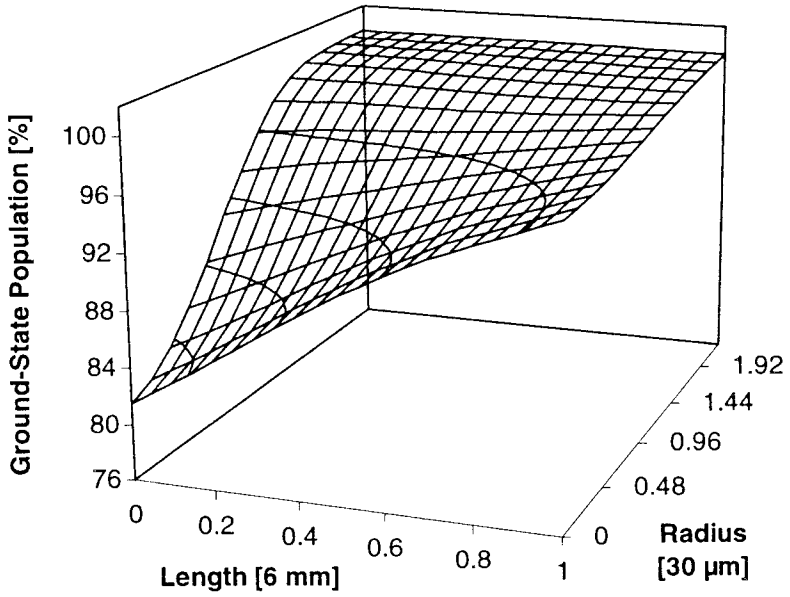
Ground-State Population [%]
100
96
92
88
84
80
76
0
0.2
0.4
0.6
0.8
1
Length [6 mm]
0
0.48
0.96
1.44
1.92
Radius
[30 µm]

Figure 4 b) **M. Pollnau et al.** **Opt. Commun.**